Chalcogenide Letters Vol. 18, No. 10, October 2021, p. 639 - 647

Direct growth of MoS_2-Ni_3S_2 core-shell nanowire array on nickel foam as a bifunctional electrode for supercapacitor and electro-oxidation of methanol

M. B. Poudel[a], A. A. Kim[b,*]
[a]*Department of Convergence Engineering Technology, Jeonbuk National University, Jeonju, South Korea*
[b]*Department of Healthcare Management, Woosong University, Daejeon, South Korea*

Herein, molybdenum sulfide-nickel sulfide (MoS_2-Ni_3S_2) core shell nanowires were directly grown on nickel foam by one step hydrothermal process. The MoS_2-Ni_3S_2 was employed as electrode for supercapacitor electrode and methanol oxidation. The MoS_2-Ni_3S_2 electrode exhibited the specific capacitance of 792 F g^{-1} at a current density of 1 A g^{-1} in a three electrode cell configuration in 1 M KOH electrolyte and maintained the current density up to 168.7 A g^{-1} in 1 M KOH electrolyte mixes with 0.5 M methanol. This work confirmed the suitability of the transition metal sulfides for energy storage and electro-oxidation of methanol.

(Received August 17, 2021; Accepted October 25, 2021)

Keywords: MoS_2-Ni_3S_2, Core-shell nanowires, Supercapacitors, Methanol oxidation

1. Introduction

With the rapidly growing energy crisis and regular worsening of the environment due to the extensive consumption of fossil fuel has collectively drawn researchers to the development of green and sustainable energy storage/conversion devices [1]. Rechargeable batteries and supercapacitors are emerging as advance energy storage device to meet the current energy demands [2, 3]. The limited charge-discharge rate and low power density can be considered as the major drawbacks for delivering high energy [4]. On the other hand, supercapacitors as green energy storage systems have multiple fascinating properties including superior power density, rapid charge-discharge process, outstanding lifecycle stability, low cost, and ease of operation [5]. Owing to the aforementioned functionalities, huge efforts have been devoted on fabricating inexpensive, multifunctional, state-of-art high performance electrode materials for supercapacitors. The commonly used electrode materials for supercapacitors include transition metal oxides/hydroxides, nitrides, phosphides, sulfides, polymers, and carbon based materials [6-11]. Especially, transition metal oxides/hydroxides are frequently used materials for redox-type supercapacitors [12]. However, they are still struggling for achieving high cycling performance and rate capabilities. Therefore, it is highly desirable to design green electrode materials with high capacitance, rate capability and conductivity on the account of volume expansion and sluggish ions diffusion during the charge-discharge process.

Transition metal dichalcogenides (TMDS) have becoming most promising electrode materials for high performance supercapacitor, owing to its good redox reaction and conductivity [13]. Among the transition metal dichalcogenides nickel sulfide (Ni_3S_2) has attracted immense attention as electrode material for SCs because of its high theoretical capacitance, oxidation-reduction reversibility, non-toxicity, abundant availability, and good metallic conductivity with resistivity of 1.8×10^{-5} Ω cm^{-1} at room temperature, providing easy transportation of electrons/ions [3, 14]. Besides, the low electronegativity of the sulfur anchors the electronic transmission easily [15, 16]. Even though, Ni_3S_2 based electrodes are used for supercapacitors, however the reports demonstrated very limited specific capacitance for supercapacitors, far from its theoretical capacitance [17]. Various studies demonstrated that the electrochemical performance of Ni_3S_2 could be enhanced by combining Ni_3S_2 with two dimensional conductive additives [13].

---

[*] Corresponding author: allisonkim@wsu.ac.kr

https://doi.org/10.15251/CL.2021.1810.639

Lie and co-workers reported flower like Ni_3S_2-CoS composite electrode with a specific capacitance of 712.12F g^{-1} at 1 A g^{-1} [18].

Another transition metal sulfide, molybdenum sulfide (MoS_2) possesses a distinct place in the field of energy storage/ conversion because of its fascinating electrochemical properties. The structure of Molybdenum sulfide (MoS_2) is similar to that of graphene, composed of three atoms (S-Mo-S) in which Mo atom is sandwiched by two S atoms through weak van der Walls attractions, similar structure to that of graphene [19]. The large spacing of the adjacent layers and weak van der Walls interactions enable the easy insertion/deinsertion of the electrolyte ions (K^+, Na^+), providing a large electroactive surface area for intercalation and transportation. In addition, the Mo ions can exhibit a wide range of oxidation states from +2 to +6, endowing its ability to the faradaic redox reaction, which significantly plays a crucial role in enhancing the electrochemical charge storage capabilities [6]. Various studies have revealed that the electrochemical properties of Ni_3S_2 can be improved by combining Ni_3S_2 and MoS_2 to form the hybrid structure [16]. However, these methods are complex, and the fabrication cost will restrict for day-to-day synthesis. Wang et al synthesized Ni_3S_2@MoS_2 nanorod array on Ni foam using P123 and achieves high capacitance[20]. The combination of 1D core and 2D shell materials simultaneously resulted high electrochemical performance. Moreover, core-shell nanostructure generally fabricated either by multistep transformation route or by using surfactant. Therefore, it is highly desirable to fabricate hierarchical core-shell nanowire arrays with well-defined morphologies and high electrochemical activities at a low fabrication cost.

Based on above considerations, in this work, MoS_2-Ni_3S_2 nanowire arrays were vertically grown on a nickel foam by one step hydrothermal process and used as electrode material for supercapacitor and electro-oxidation of methanol. The MoS_2-Ni_3S_2 electrode showed the enhanced charge storage capacity than pure Ni_3S_2. The MoS_2 and Ni_3S_2 both participate in the electrochemical activities. Their synergistic effect can enhance the materials conductivity and the MoS_2 shell can provide more driving force for the redox kinetics. Therefore, we thought it is worthwhile to prepare the MoS_2-Ni_3S_2 core shell nanowire and explore it as an effective electrode material for supercapacitor and methanol oxidation.

2. Experimental

2.1. Material synthesis

MoS_2-Ni_3S_2 nanowire arrays were prepared using simple one-step hydrothermal process. In detail, 1 mM of sodium molybdate dihydrate ($Na_2MoO_4.2H_2O$, Sigma Aldrich, USA) was dissolved in mixture of ethanol (10 mL) and ultrapure water (40 mL) and stirred for 30 minutes. 6 mM of thiourea ((NH_2CSNH_2, SAMCHUN, Korea) was added to the solution with constant stirring for 30 minutes to get the homogenous solution. A pre-cleaned nickel foam (2 cm x 3 cm, Goodfellow) was immersed into the solution and transferred to the autoclave and heated at 160 ^oC for 10 hours. After the autoclave was cooled down to room temperature, the nickel foam was rinsed with ultrapure water and ethanol subsequently and then dried in a vacuum oven for 14 hours at 60 ^oC. Pure Ni_3S_2 nanowire was also prepared by similar process without adding $Na_2MoO_4.2H_2O$.

2.2. Electrochemical measurements

The electrochemical workstation (Zieve SP2) was used to perform the electrochemical measurements of the prepared electrode at room temperature. The prepared electrode (1 cm^2) is directly used as working electrode while the Ag/AgCl (saturated KCl) and platinum wire was used as reference electrode and counter electrode, respectively. The electrochemical measurements were conducted in 1 M KOH solution. Cyclic voltammetry (CV) and galvanostatic charge discharge test were carried out to understand the oxidation-reduction behavior of the electrodes. Electrochemical impedance spectroscopy (EIS) was recorded at frequencies ranging from 0.01 Hz to 100 kHz with the potential amplitude of 5 mV. The specific capacitance of the electrodes was calculated using GCD curve by using given equation[10]:

$$Specific\ capacitance\ (C_{sp}) = \frac{I \times \Delta t}{m \times \Delta v}$$

where, I (A), Δt (sec), m (g), and Δv (V) are the charge discharge current, discharge time, active mass of electrodes, and operating potential voltage, respectively. The electrocatalytic activities of MoS_2-Ni_3S_2 electrode towards electro-oxidation of methanol were analyzed by CV, chronoamperometry and EIS techniques at room temperature using 1 M KOH and (0.5 M methanol + 1 M KOH) as electrolytes in standard three electrode cell configuration.

3. Result and discussion

3.1. Morphological and structural study

Scheme 1 illustrates the formation of MoS_2-Ni_3S_2 nanowire array on the Ni foam. The Ni foam not only acted as a template but also provide nickel source for the growth of Ni_3S_2. During the reaction, sulfur ions are released from thiourea, which react with the exposed Ni surface to form Ni_3S_2 nanowire, and in the presence of MoO_4^- ions, it produce MoS_2 nanosheets according to the following equation [20, 21].

$$NH_2CSNH_2 + H_2O \rightarrow 2NH_3 + 2H_2S + CO_2$$
$$3Ni + 2H_2S \rightarrow Ni_3S_2 + H_2$$
$$MoO_4^- + 3H_2S \rightarrow MoS_2 + 3H_2 + SO_4^-$$

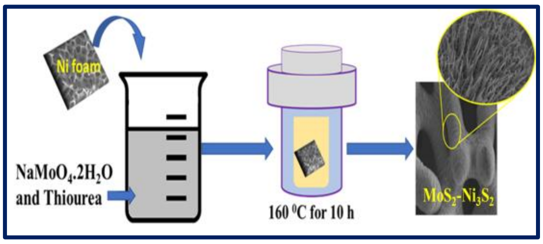

Scheme 1. Schematic representation for the synthesis of MoS_2-Ni_3S_2 nanowire on Ni-foam.

The morphology and detailed crystallographic structure of the samples were studied by field-emission scanning electron microscopy (FE-SEM, Hitachi S 7400, Japan, 200 kV) and transmission electron microscopy (TEM, JEM-2200, JEOL, Japan). Figure 1 (a), and (b) shows the dense and vertically aligned Ni_3S_2 nanowire are grown uniformly on the Ni-foam with a diameter of 60 nm and several micrometers in length. The FE-SEM image (Figure 1 (c) and (d)) of MoS_2-Ni_3S_2 displayed that uniform thin sheet of MoS_2 were formed on the vertically aligned Ni_3S_2 nanowire. The diameter of Ni_3S_2 nanowire is slightly reduced on the presence of Mo precursor, this might be due to the etching effect of Mo ions. A close look to the FE-SEM image of MoS_2-Ni_3S_2 displays the uniform coverage of MoS_2 nanosheets on Ni_3S_2 nanowires forming core shell structure (inset of Figure 1 (d)). The FE-SEM elemental distribution x-ray spectroscopy (EDX) mapping and corresponding spectra presented in Figure 1 (e) and (f), revealed the distribution of Ni, Mo, and S elements uniformly. For the detailed study of the compositional and crystallographic structure of MoS_2-Ni_3S_2 nanowire array on Ni foam, the MoS_2-Ni_3S_2 were separated from Ni foam by sonication and analyzed by TEM technique. The TEM image (Figure 2 (a) and (b)) depicts that the Ni_3S_2 nanowires were wrapped uniformly by thin sheets, forming hierarchical core-shell structure, consistent to FE-SEM results. Such type of structure is favorable for increasing the active surface area of electrodes and anchored the electrochemical performances. Figure 2 (c) shows the HR-TEM image of MoS_2-Ni_3S_2 nanowire obtained from the yellow dotted region. The lattice spacing in the HR-TEM were determined to be 0.28 nm for the nanowire core and 0.27 nm for the nanosheets shell, which corresponds to the (110) planes of Ni_3S_2 and (100) planes of MoS_2, respectively [22]. The SAED pattern corresponds the nature of Ni_3S_2-MoS_2

composites. Furthermore, the TEM EDX color mapping reveals evenly distributed Ni, Mo, and S elements, confirming the formation of MoS_2-Ni_3S_2 hierarchical core shell structure. The phase purity and crystal structure of Ni-foam, Ni_3S_2 and MoS_2-Ni_3S_2 were studied by X-ray diffraction (XRD, Rigaku Co., Japan, Cu Kα, $\lambda = 1.540$ Å, 30 kV, 40 mA) analysis and presented in Figure 3. The pristine Ni foam shows high intensity crystalline diffraction peaks pointed $2\theta = 44.6^0$, 52^0 and 76.2^0 [23]. In the XRD pattern of Ni_3S_2 depicts well-defined diffraction peaks at 21.76, 31.1, 37.79, 49.72, 55.3, and 73.51 corresponds to the (101), (110), (003), (113), (300), and (312) planes of heazlewoodite Ni_3S_2 (JCPDS card No.071-1682) [24]. As seen in the XRD pattern of the MoS_2-Ni_3S_2, additional peaks at 33.3, 35.8, 39, and 58.5 are clearly distinct, which is related to the (100), (102), (103), and (110) planes of MoS_2 (JCPDS No. 37-1492) [25]. Additionally, the peak intensity of Ni_3S_2 phase decreases slightly due to the formation of thin MoS_2 nanosheets on the surface of Ni_3S_2 nanowires.

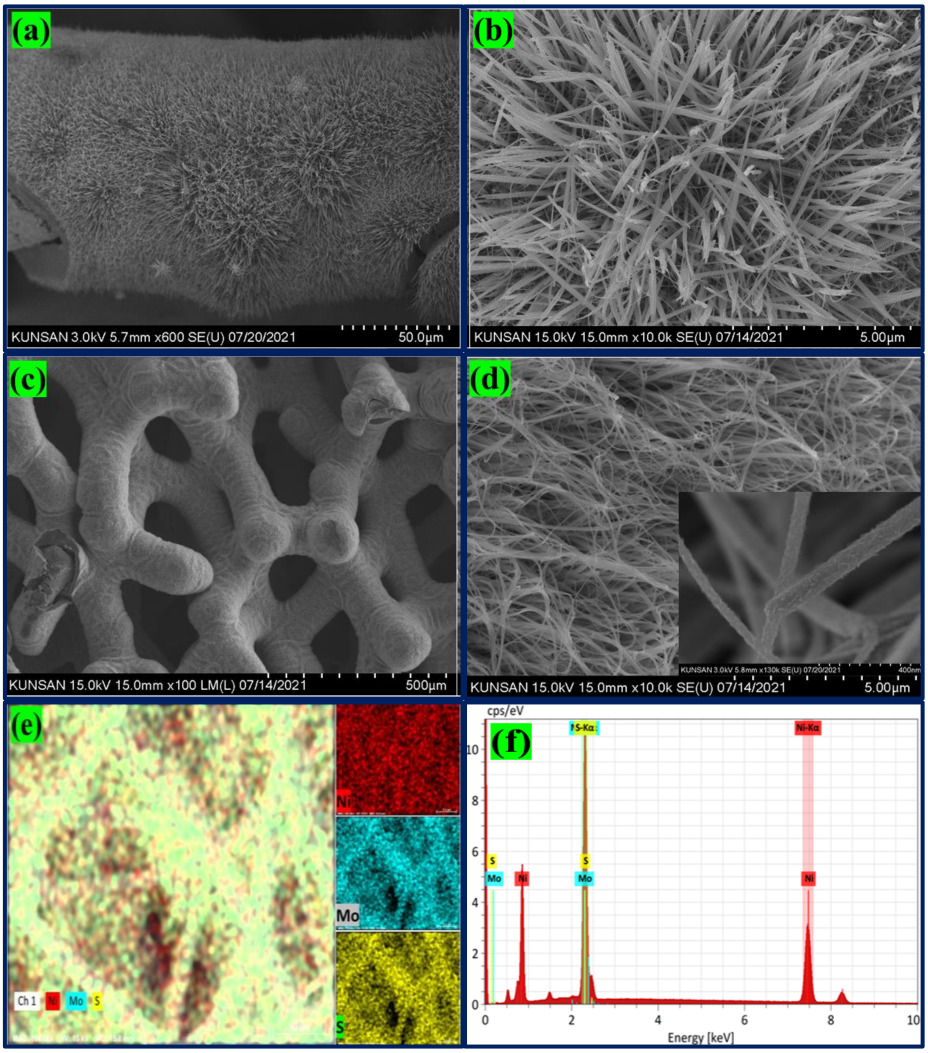

Fig. 1. FE-SEM image of Ni_3S_2 ((a) and (b)) and MoS_2-Ni_3S_2 ((c) and (d)) grown on Ni-foam at different magnification, (e) EDX colour mapping of MoS_2-Ni_3S_2 and (f) corresponding EDX spectrum.

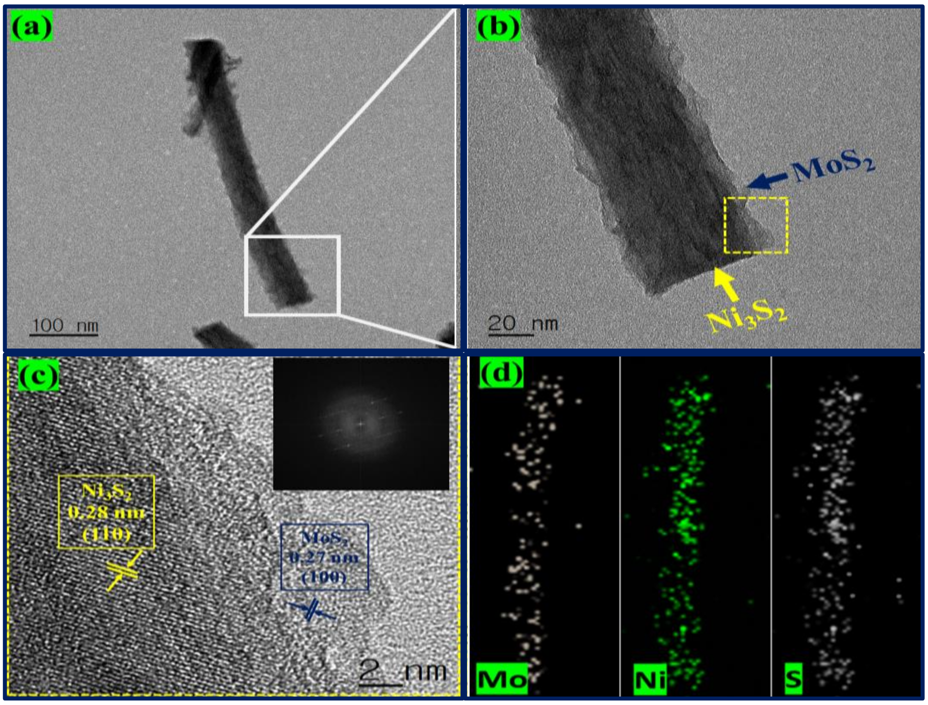

Fig. 2. (a), (b) TEM and HR-TEM images of MoS_2-Ni_3S_2 at various resolution (inset of c; SAED pattern) and (d) TEM-EDX elemental distribution of Mo, Ni and S.

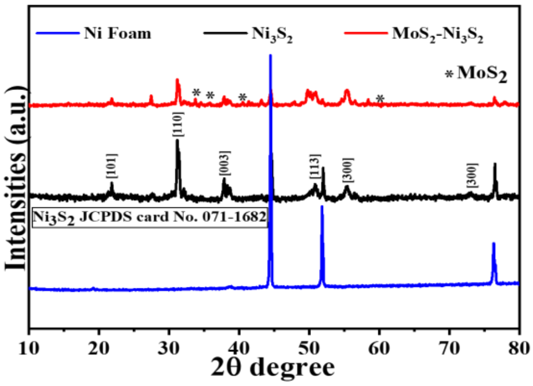

Fig. 3. XRD patterns of bare Ni foam, Ni_3S_2 and MoS_2-Ni_3S_2.

3.2. Electrochemical performance

The electrochemical performance of the electrodes was studied in a three electrode cell configuration using CV, GCD and EIS in 1 M KOH solution. The CV was performed within a potential window of 0 to 0.6 V. Figure 4 (a) shows the CV profiles of Ni_3S_2 and MoS_2-Ni_3S_2 electrodes at the scan rates of 10 mV s^{-1}, and evidently, both CV curves contains a pair of current peaks. The redox peaks present in the CV curves suggests that the capacitance performance of these electrodes is primarily governed by the pseudocapacitive process, being characteristic reversible faradaic transition between the redox couples of MoS_2-Ni_3S_2 as following reaction [26, 27].

$$Ni_3S_2 + 3OH^- \leftrightarrow Ni_3S_2(OH)_3 + 3e^-$$
$$MoS_2 + K^+ + e^- \leftrightarrow MoS\text{-}SK$$

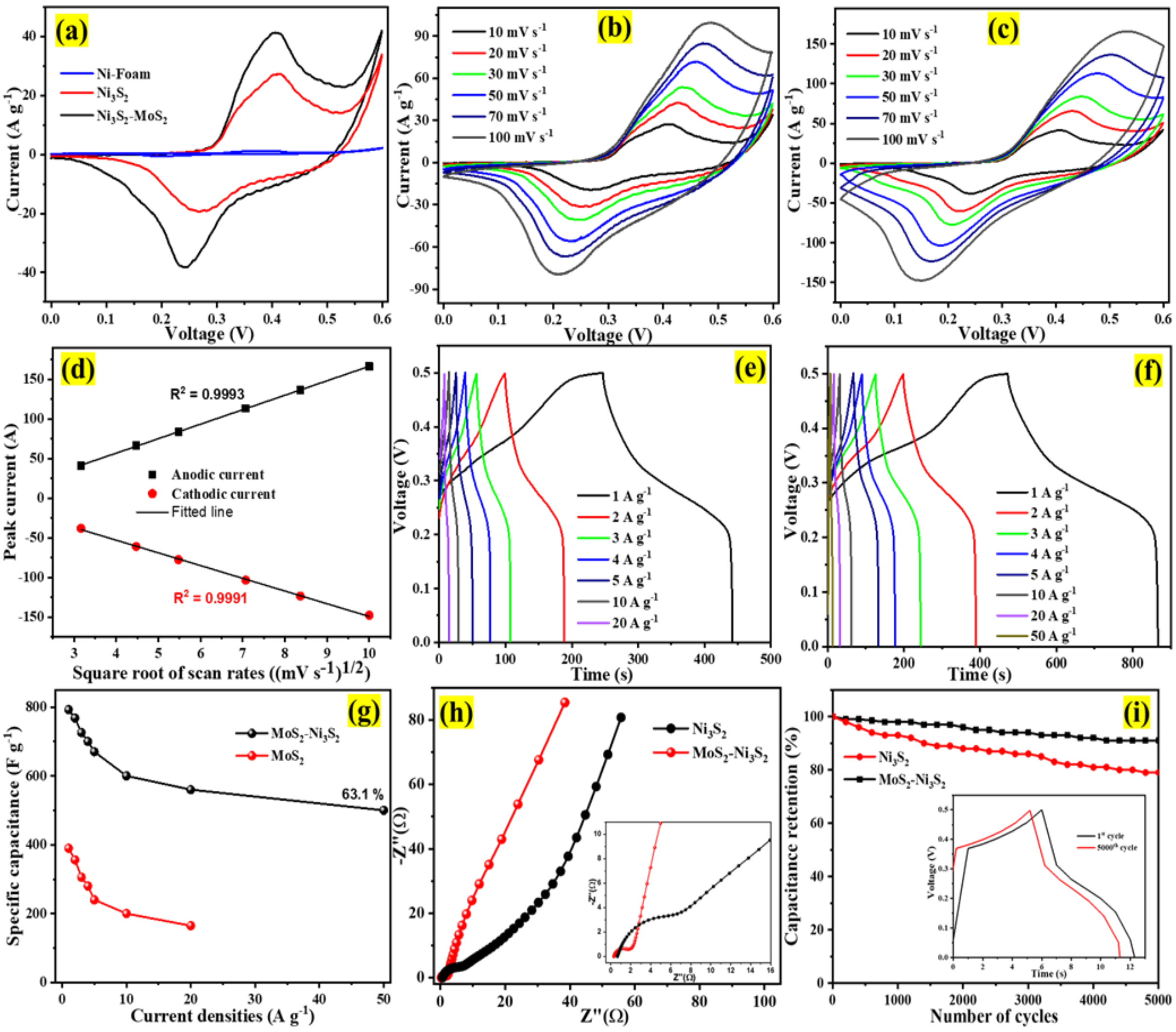

Fig. 4. (a) CV curves of Ni-foam, Ni_3S_2 and MoS_2-Ni_3S_2 electrode at 10 mV s^{-1}, CV curves of (c) Ni_3S_2 and (d) MoS_2-Ni_3S_2 at various scan rates, (d) variation of current response with respect to square root of scan rates, GCD curves of (e) Ni_3S_2, (f) MoS_2-Ni_3S_2 at various current density, (g) specific capacitance of electrode at different current densities, (h) Nyquist plot of both electrodes (inset; shows the magnified Nyquist plots at high frequency region), and (i) cyclic stability of both electrodes (inset; initial and final GCD curves).

The MoS_2-Ni_3S_2 electrode exhibited higher CV enclosed area than that of the pure Ni_3S_2, reveling the enhancement of its capacitance. Figure 4 (b) and (c) depicts the CV curves of the Ni_3S_2 and MoS_2-Ni_3S_2 electrodes, respectively. MoS_2-Ni_3S_2 electrode still preserved a similar at various scan rates from 10 mV s^{-1} to 100 mV s^{-1}. However, the peak current shift towards opposite potential with the increase in the scan rates due to the partial intercalation and deintercalation of the electrolyte ions at higher scan rates. As shown in the Figure 4 (d) the linear relationship between the peak current and square root of scan rates revealed the redox reaction on the electrode is controlled by the ion diffusion process [28]. Figure 4 (e), and (f) presents GCD curves of Ni_3S_2 and MoS_2-Ni_3S_2 electrodes at various current densities within the operational potential ranges from 0 to 0.5 V. The symmetric charge discharge curves showed excellent reversibility in the redox process, which is consistent to the CV results. It is clear that the MoS_2-Ni_3S_2 electrode demonstrates longer discharge time implying higher specific capacitance than Ni_3S_2. The specific capacitance of both electrodes at various current densities were computed from their GCD curves. As expected, the MoS_2-Ni_3S_2 exhibit the high specific capacitance of 792 F g^{-1} at 1 A g^{-1}, and even retains 500 at high current density of 50 A g^{-1} (nearly 63 % of its initial capacitance) (Figure 4 (g)).

Whereas the Ni_3S_2 alone exhibit lower specific capacitance of 390 at 1A g^{-1} and only 42.30 % of its initial capacitance was retained at 20 A g^{-1}. The introduction of MoS_2 significantly improves the specific capacitance and rate capability. On the contrary, the MoS_2-Ni_3S_2 electrode proclaims the utility of thin MoS_2 nanosheets to form more exfoliated and porous morphologies. This more exposed electroactive sites in the MoS_2-Ni_3S_2 electrode helps to channelizing electron/ions in efficient manner ameliorating the kinetics of the redox reaction and hence the capacitive performance of the MoS_2-Ni_3S_2 electrode.

To aim the deeper insight into the charge transfer behavior of the prepared electrodes EIS was conducted and corresponding Nyquist plot of both electrodes are illustrated in Figure 4 (h). Obviously, the Nyquist curves are composed of a semicircular at the high frequency region and oblique line in the lower frequency region. The semicircular region at higher frequency region represents the charge transfer resistance associated with faradaic reaction whereas the inclined line in the lower frequency region represents diffusion resistance [26, 29]. As displayed in inset of Figure 4 (h), MoS_2-Ni_3S_2 electrode exhibit smaller arc diameter at higher frequency zone with upward deviation in the lower frequency region than Ni_3S_2, which suggest that the assembly of MoS_2 nanosheets on Ni_3S_2 nanowire on Ni foam could enhance the conductivity of complete system. Long term cyclic stability of the electrode is important factor for the practical application. The cycle life of the electrodes was executed over 5000 charge discharge cycles at 50 A g^{-1} (Figure 4(i)). The hierarchical MoS_2-Ni_3S_2 core-shell electrode exhibits superior cyclic performance of 91 % of its initial capacitance after 5000 cycles, which is higher than Ni_3S_2 electrode (79 % of its initial capacitance was maintained). The electrochemical performance of as prepared MoS_2-Ni_3S_2 is superior to the previously reported works [30-33].

The superior electrochemical performance of the hierarchical MoS_2-Ni_3S_2 core-shell electrode could be ascribed to the following reasons: (a) the highly conductive Ni_3S_2 core nanowire endows the quick transportation of the electrons to the conductive substrate, (b) the void space between the MoS_2 nanosheets and Ni_3S_2 nanowires can serve as ion bank to facilitate the electrolyte ion transfer and protect, (c) the ultrathin layered MoS_2 not only allow the easy transportation of electrolyte ions to the core but also protect the core nanowire from electrolyte dissolution during the charge-discharge process and results high efficiency of the electrodes, and (d) most importantly the direct growth of the MoS_2-Ni_3S_2 hierarchical core-shell nanowire array on conductive Ni foam with no adhesive guarantee close contact between active material and current collector, in favor of electron transfer during redox reaction.

3.3. Electrocatalytic performance of MoS_2-Ni_3S_2 for methanol oxidation

The electrolytic methanol oxidation by MoS_2-Ni_3S_2 has been studied in detail for the first time. Figure 5 (a) displays the CV curves of MoS_2-Ni_3S_2 in 1 M KOH with and without 0.5 M methanol at 50 mV s^{-1}. It is already discussed that the MoS_2-Ni_3S_2 electrode displays distinct redox peaks in 1 M KOH electrolyte, which may provide enough electroactive sites for methanol oxidation. However, after the addition of 0.5 M methanol, the MoS_2-Ni_3S_2 electrode exhibit dissimilar and intense sharp end toward higher potential. The increase in anodic current response with the addition of methanol suggests the electrocatalytic oxidation behavior of the MoS_2-Ni_3S_2 towards methanol [12]. Figure 5 (b) shows the chronoamperometric (CA) profile of MoS_2-Ni_3S_2 obtained. A steady decay in the current density (188 A g^{-1} to 175.5 A g^{-1}) was observed for first 500 s and remains almost constant for 2000 s, which might be attributed to the accumulation of intermediate product originated during the adsorption and desorption of methanol towards the surface of electrodes [17]. Nevertheless, the MoS_2-Ni_3S_2 electrode still delivered 89.36 % of retention in current response suggesting the admirable stability towards electrocatalytic oxidation of methanol. The long term stability of MoS_2-Ni_3S_2 electrode was further investigated by recording CV curves (Figure 5 (c)) for 500 continuous cycles (in 1 M KOH + 0.5 M methanol) at 50 mV s^{-1}. This reveals that the voltammogram is fairly stable even after 500 cycles. The charge transfer resistance of the MoS_2-Ni_3S_2 electrode was inspected by the EIS measurements carried out in pure 1 M KOH and 1 M KOH + 0.5 M methanol electrolytes recorded at 5 mV within the frequency range of 0.01 Hz to 100 kHz. Figure 5 (d) represent the Nyquist plot of for both electrolytes. The smaller semicircle can be observed in both electrolytes, indicating a smaller charge transfer resistance between the electrolytes and electrode materials. The MoS_2-Ni_3S_2 exhibit the superior electrochemical performances and anti-poisoning ability towards methanol. This can be attributed to its robust structural stability and availability of abundant electroactive sites.

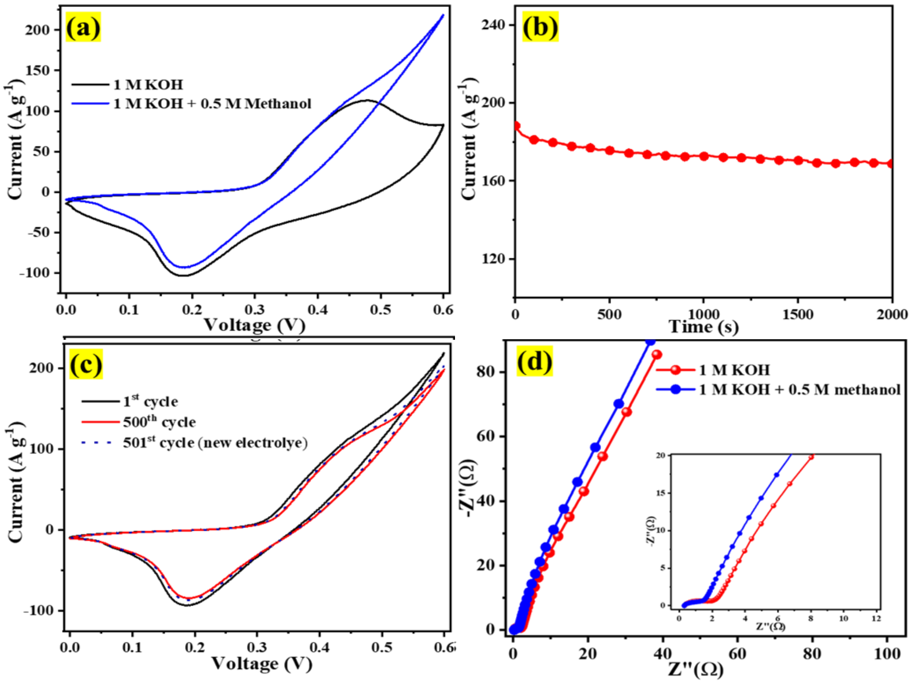

Fig. 5. (a) CV curves of MoS_2-Ni_3S_2 in 1 M KOH and (1 M KOH + 0.5 M methanol) electrolytes at 10 mV s^{-1}, (b) chronoamperometric curve of MoS_2-Ni_3S_2 electrode in (1 M KOH + 0.5 M methanol) electrolyte, (c) CV curves of MoS_2-Ni_3S_2 electrode at 10 mV s^{-1} in the 1 M KOH + 0.5 M methanol) electrolyte for different number of cycles, and (d) EIS of MoS_2-Ni_3S_2 electrode in both electrolytes.

4. Conclusions

In summary, we have successfully synthesized MoS_2-Ni_3S_2 core shell nanowire arrays by one step hydrothermal process. Benefiting from the synergetic effect of ultrathin MoS_2 nanosheets and Ni_3S_2 nanowire directly grown in Ni foam, it showed good electrochemical performance in supercapacitor and methanol oxidation. The MoS_2-Ni_3S_2 electrode delivered excellent specific capacitance of 792 F g^{-1} at 1 A g^{-1} with high rate capability and longer life cycle. Additionally, the prepared MoS_2-Ni_3S_2 electrode showed admirable electro-oxidation activity and electro-oxidation stability.

The porous and uniform nanostructure formed by the combination of thin MoS_2 nanosheets and Ni_3S_2 nanowire provides sufficient ion/electron diffusion channel and effective contact area, endowing excellent conductivity, thus greatly facilitated easy transfer if ions within the electrode. The overall results suggested that the MoS_2-Ni_3S_2 can be used as potential electrode material for supercapacitor and oxidation of methanol.

References

[1] T. Liu, L. Zhang, B. Cheng, J. Yu, Advanced Energy Materials **9**, 1803900 (2019).
[2] M. B. Poudel, C. Yu, H. J. Kim, Catalysts, 10 (2020).
[3] B. Pant, G. P. Ojha, M. Park, Journal of Energy Storage **32**, 101954 (2020).
[4] J. Li, S. Luo, B. Zhang, J. Lu, W. Liu, Q. Zeng, J. Wan, X. Han, C. Hu, Nano Energy **79**, 105410 (2021).
[5] X. Li, W. Yan, S. Guo, Y. Liu, J. Niu, L. Yin, Z. Wang, Electrochimica Acta **387**,

138488 (2021).
[6] X. Zhang, R. Zhao, Q. Wu, W. Li, C. Shen, L. Ni, H. Yan, G. Diao, M. Chen, ACS Nano **11**, 8429 (2017).
[7] J. Theerthagiri, R. A. Senthil, P. Nithyadharseni, S. J. Lee, G. Durai, P. Kuppusami, J. Madhavan, M. Y. Choi, Ceramics International **46**, 14317 (2020).
[8] B. Pant, G.P. Ojha, J. Acharya, M. Park, International Journal of Hydrogen Energy **46**, 2774 (2021).
[9] M. Babu Poudel, H. Joo Kim, Journal of Energy Chemistry, (2021).
[10] M. B. Poudel, M. Shin, H. J. Kim, International Journal of Hydrogen Energy **46**, 474 (2021).
[11] Y. Qin, Y. Lyu, M. Chen, Y. Lu, P. Qi, H. Wu, Z. Sheng, X. Gan, Z. Chen, Y. Tang, Electrochimica Acta, 139059 (2021).
[12] J. Acharya, B. Pant, G.P. Ojha, H.-S. Kong, M. Park, Journal of Colloid and Interface Science **602**, 573 (2021).
[13] R. Fan, J. Zhou, W. Xun, S. Cheng, S. Vanka, T. Cai, S. Ju, Z. Mi, M. Shen, Nano Energy **71**, 104631 (2020).
[14] Y. Ouyang, Y. Chen, J. Peng, J. Yang, C. Wu, B. Chang, X. Guo, G. Chen, Z. Luo, X. Wang, Journal of Alloys and Compounds **885**, 160979 (2021).
[15] R. Gao, Q. Zhang, F. Soyekwo, C. Lin, R. Lv, Y. Qu, M. Chen, A. Zhu, Q. Liu, Electrochimica Acta, **237**, 94 (2017).
[16] Y.-Z. Xu, C.-Z. Yuan, X.-P. Chen, Journal of Solid State Chemistry **256**, 124 (2017).
[17] Y. Cheng, M. Zhai, J. Hu, Applied Surface Science **480**, 505 (2019).
[18] J. H. Zheng, R. M. Zhang, X. G. Wang, Materials Letters **228**, 191 (2018).
[19] G. P. Awasthi, S. P. Adhikari, S. Ko, H. J. Kim, C. H. Park, C. S. Kim, Journal of Alloys and Compounds **682**, 208 (2016).
[20] J. Wang, D. Chao, J. Liu, L. Li, L. Lai, J. Lin, Z. Shen, Nano Energy **7**, 151 (2014).
[21] L. Li, H. Yang, J. Yang, L. Zhang, J. Miao, Y. Zhang, C. Sun, W. Huang, X. Dong, B. Liu, Journal of Materials Chemistry A **4**, 1319 (2016).
[22] J. Gao, X. Wang, X. Wang, R. Que, Y. Fang, B. Shi, Z. Wang, RSC Advances **6**, 68460 (2016).
[23] X. Li, D. Li, L. Qiao, X. Wang, X. Sun, P. Wang, D. He, Journal of Materials Chemistry **22**, 9189 (2012).
[24] M. Kumar, D.I. Jeong, N. Sarwar, D. H. Yoon, Ceramics International **47**, 16852 (2021).
[25] A. Muthurasu, G. P. Ojha, M. Lee, H. Y. Kim, Electrochimica Acta **334**, 135537 (2020).
[26] Y. He, D. Liu, H. Zhao, J. Wang, Y. Sui, J. Qi, Z. Chen, P. Zhang, C. Chen, D. Zhuang, Journal of Energy Storage **41**, 103003 (2021).
[27] M. B. Poudel, H. P. Karki, H. J. Kim, Journal of Energy Storage **32**, 101693 (2020).
[28] G. P. Ojha, B. Pant, S.-J. Park, M. Park, H.-Y. Kim, Journal of Colloid and Interface Science **494**, 338 (2017).
[29] J. Wang, T. Park, J. W. Yi, B. Ding, J. Henzie, Z. Chang, H. Dou, X. Zhang, Y. Yamauchi, Nanoscale Horizons **4**, 526 (2019).
[30] W. Niu, Z. Xiao, Z. Zhao, S. Zhai, N. Liu, C. Qin, Journal of Alloys and Compounds **885**, 161194 (2021).
[31] S. Silambarasan, T. Maiyalagan, Materials Letters **299**, 130075 (2021).
[32] A. Sun, L. Xie, D. Wang, Z. Wu, Ceramics International **44**, 13434 (2018).
[33] S. Qin, T. Yao, X. Guo, Q. Chen, D. Liu, Q. Liu, Y. Li, J. Li, D. He, Applied Surface Science **440**, 741 (2018).